

Lewis Acids

Slow Reactant–Water Exchange and High Catalytic Performance of Water-Tolerant Lewis Acids

Yusuke Koito,^[a, b] Kiyotaka Nakajima,^[a, c] Hisayoshi Kobayashi,^[d] Ryota Hasegawa,^[d] Masaaki Kitano,^[e] and Michikazu Hara^{*[a, f]}

Abstract: ³¹P nuclear magnetic resonance (NMR) spectroscopic measurement with trimethylphosphine oxide (TMPO) was applied to evaluate the Lewis acid catalysis of various metal triflates in water. The original ³¹P NMR chemical shift and line width of TMPO is changed by the direct interaction of TMPO molecules with the Lewis acid sites of metal triflates. [Sc(OTf)₃] and [In(OTf)₃] had larger changes in ³¹P chemical shift and line width by formation of the Lewis acid–TMPO complex than other metal triflates. It originates from the strong interaction between the Lewis acid and TMPO, which results in higher stability of [Sc(OTf)₃TMPO]

and [In(OTf)₃TMPO] complexes than other metal triflate–TMPO complexes. The catalytic activities of [Sc(OTf)₃] and [In(OTf)₃] for Lewis acid-catalyzed reactions with carbonyl compounds in water were far superior to the other metal triflates, which indicates that the high stability of metal triflate–carbonyl compound complexes cause high catalytic performance for these reactions. Density functional theory (DFT) calculation suggests that low LUMO levels of [Sc(OTf)₃] and [In(OTf)₃] would be responsible for the formation of stable coordination intermediate with nucleophilic reactant in water.

Introduction

Lewis acids, represented by AlCl₃, BF₃, and SnCl₄, involve a metal center as an electron pair acceptor that accepts the electron pair from a nucleophile,^[1] and are effective catalysts for carbon–carbon bond-forming reactions in organic solvents.^[2] Lewis acids are essential catalysts used for the production of indispensable chemicals, including polymers, medicines, and agricultural chemicals. However, the rationale for the reac-

tivity of Lewis acids has remained vague: Lewis acid catalysis, due to both the energy levels of the highest occupied molecular orbital (HOMO) of the reactant (nucleophile) and the lowest unoccupied molecular orbital (LUMO) of the Lewis acid (electrophile),^[1] is more complicated than that for Brønsted acids, which can be discussed with respect to acid strength, such as the Hammett acidity function, *H*₀. Although most Lewis acids are decomposed or deactivated in water, metal trifluoromethanesulfonates (triflates) ([M(OTf)_x]; M: metal center, OTf: –OSO₂CF₃) are well known as the few exceptions that function in water for various reactions, including the Mukaiyama aldol condensation of various carbonyl compounds with silyl enol ethers.^[3,4] [Sc(OTf)₃] and scandium tris(dodecylsulfate) exhibit particularly high catalytic performance for the Mukaiyama aldol condensation, Mannich-type reaction, Friedel–Crafts alkylation, and allylation reactions as water-compatible Lewis acid catalysts.^[5] These homogeneous Lewis acids can activate the carbonyl group of a reactant even in water; electrophilic attack of the evolved carbocation intermediate then results in the desired product of these reactions.^[6] Although a wide variety of metal triflates have been recognized as active Lewis acid catalysts in water,^[3] the catalytic performance of these metal triflates is strongly dependent on the metal species. Kobayashi et al. reported that the catalytic activities of many metal chlorides, perchlorides, and triflates for the Mukaiyama-aldol reaction are related to their hydrolysis constants (p*K*_h) and water exchange rate constants (WERC).^[7] The hydrolysis constant reflects the stability of metal salts in water; metal salts with small p*K*_h are easily decomposed in water into the corresponding metal hydroxides, whereas metal salts with large p*K*_h exhibit less interaction with electrophilic molecules, including water,

[a] Y. Koito, Dr. K. Nakajima, Prof. M. Hara
Materials and Structures Laboratory
Tokyo Institute of Technology
Nagatsuta, Midori-ku Yokohama 226-8503 (Japan)
E-mail: mhara@mssl.titech.ac.jp

[b] Y. Koito
Research Fellow of Japan Society
for the Promotion of Science (JSPS)
5-3-1 Chiyoda-ku, Tokyo 102-0083 (Japan)

[c] Dr. K. Nakajima
Japan Science and Technology (JST) Agency, PRESTO
4-1-8 Honcho, Kawaguchi 332-0012 (Japan)

[d] Prof. H. Kobayashi, R. Hasegawa
Department of Chemistry and Materials Technology
Kyoto Institute of Technology
Matsugasaki, Sakyo-ku, Kyoto 606-8585 (Japan)

[e] Dr. M. Kitano
Materials Research Center for Element Strategy
Tokyo Institute of Technology
Nagatsuta, Midori-ku, Yokohama 226-8503 (Japan)

[f] Prof. M. Hara
Japan Science and Technology (JST) Agency, ALCA
4-1-8 Honcho, Kawaguchi 332-0012 (Japan)

Supporting information for this article is available on the WWW under <http://dx.doi.org/10.1002/chem.201400240>.

which results in no catalytic activity. In addition, the WERC is an important factor that characterizes the Lewis acid catalytic activity. A Lewis acid with a large WERC value can facilitate the exchange of water molecules and hydrate the Lewis acid for other nucleophilic molecules, including reactants with carbonyl groups, and can thereby exhibit high catalytic activity. Tsuruta et al. reported that the catalytic activities of rare-earth metal triflates are also dependent on their competitive dissociation intensity, which was evaluated by using tandem mass spectroscopy.^[8] In addition, Wang et al. suggested that the metal triflate including the smaller metallic cation radius results in higher catalytic performance for sugar conversion due to the stronger interaction between metal cations and substrates.^[9] Although catalysis with these Lewis acids can be comprehensively discussed using these factors, they do not provide information on the direct interaction of Lewis acid sites with nucleophilic molecules in water.

In this study, the correlation of Lewis acidity with catalytic activity for some metal triflates in water was investigated by using ³¹P nuclear magnetic resonance (NMR) spectroscopy with trimethylphosphine oxide (TMPO) as a basic probe molecule. ³¹P NMR Spectroscopic measurements with trimethylphosphine (TMP) and TMPO have been widely applied to characterization of the type of acid (Brønsted and Lewis) and the strength of acid sites on solid surfaces.^[10] The 100% natural abundance of ³¹P and a large chemical shift range over 430 ppm gives the ³¹P NMR spectroscopic technique a clear advantage over ¹H and ¹³C NMR spectroscopy for the characterization of solid acid catalysts with small acid site density.^[11] Highly sensitive TMP is generally applicable to the characterization of Lewis acidity; however, TMP adsorbed on a solid surface is easily oxidized into TMPO, even in the presence of a small amount of oxidant, such as O₂. In addition, evaluation of Lewis acidity with TMP is only reliable for Lewis acids with the same metal center.^[12] Yang et al. applied liquid-state ³¹P NMR spectroscopy with TMPO to evaluate the acid strength of various homogeneous Brønsted acid catalysts and revealed that the ³¹P NMR chemical shift of TMPO reflects the Brønsted acid strength.^[13] TMPO is also expected to be an excellent probe molecule for evaluation of the Lewis acidity of metal triflates in water. The formation of a TMPO–Lewis acid complex is based on coordination of the oxygen atom on TMPO with the metal species in the Lewis acid. The phosphoryl group in TMPO is similar to the carbonyl group in various reactants, so that ³¹P NMR spectroscopy for a TMPO-coordinated Lewis acid would reflect the Lewis acid catalysis for carbonyl compounds. Here, various metal triflates with TMPO in water were examined using ³¹P NMR spectroscopy, and the correlation of Lewis acidity with the catalytic activity for the hydride transfer of pyruvic aldehyde into lactic acid and the allylation of benzaldehyde with tetraallyl tin in water is discussed.

Results and Discussion

Catalytic activity of metal triflates

The catalytic activity of various metal triflates was examined for the hydride transfer of pyruvic aldehyde into lactic acid and the allylation of benzaldehyde with tetraallyl tin in water. The former is a key reaction for the conversion of 1,3-dihydroxyacetone and glyceraldehyde into lactic acid,^[14–18] because 1,3-dihydroxyacetone and glyceraldehyde are oxidative products derived from glycerol, a byproduct of the oil and fat industry.^[19] Lewis acids have been reported as effective catalysts for the hydride transfer of glucose into fructose and pyruvic aldehyde

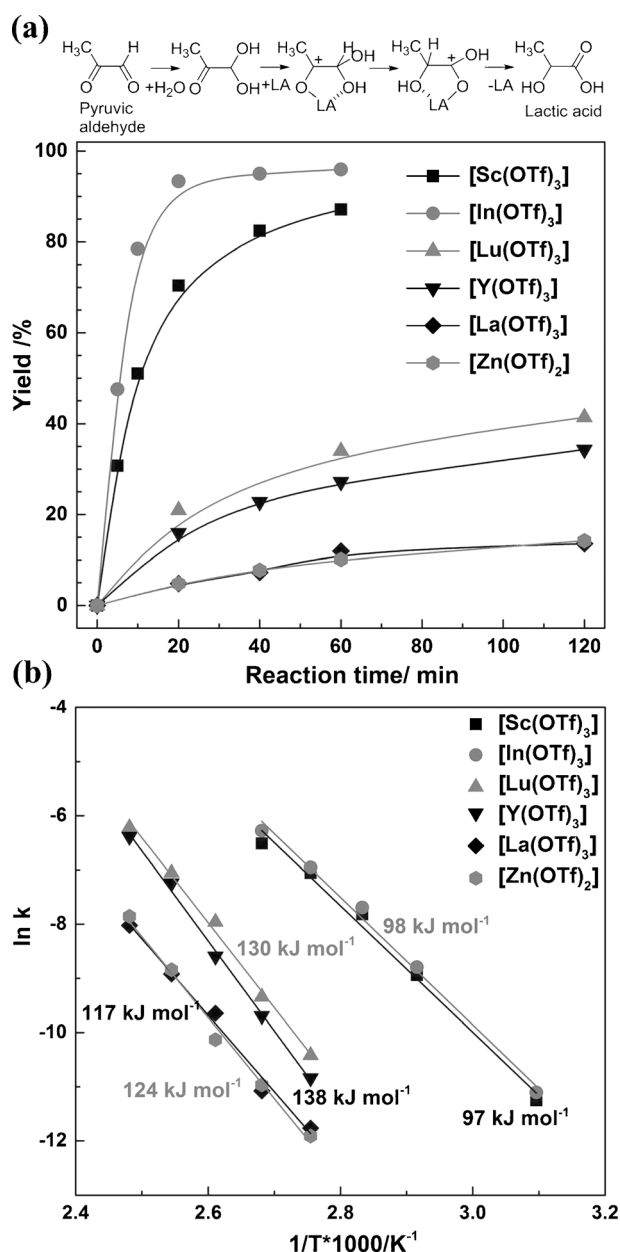


Figure 1. a) Time course for lactic acid formation over metal triflate catalysts at 383 K; b) Arrhenius plot for lactic acid formation with metal triflates in the temperature range of 323–403 K. Reaction conditions: Catalyst (0.1 mmol), 0.1 M aqueous pyruvic aldehyde (2.0 mL).

into lactic acid in water through the Meerwein–Ponndorf–Verley (MPV) reduction mechanism.^[20,21] Figure 1 (a) shows time courses for the lactic acid yield from pyruvic aldehyde over various metal triflates at 383 K. Lactic acid was not produced without an acid catalyst and Brønsted acids exhibit much poorer catalytic performance than water-tolerant Lewis acid catalysts, including metal triflates, at 383 K.^[21] [Sc(OTf)₃] and [In(OTf)₃] effectively convert pyruvic aldehyde into lactic acid, even in water; the lactic acid yields of these catalysts exceed 85% within 1 h. In contrast, [Lu(OTf)₃], [Y(OTf)₃], [La(OTf)₃], and [Zn(OTf)₂] exhibit only moderate activity for the reaction, and the lactic acid yields with these triflates are only 10–35% after 1 h. Figure 1 (b) shows Arrhenius plots and apparent activation energies (E_a) for lactic acid formation with each triflate. The formation rates of lactic acid in the early stage of the reaction (yield < 30%) and at various temperatures (323–403 K) were used for E_a estimation. Activation energies for [Sc(OTf)₃] and [In(OTf)₃] were estimated to be 97 and 98 kJ mol⁻¹, respectively, which is smaller than other metal triflates. Therefore, the high catalytic performance of [Sc(OTf)₃] and [In(OTf)₃] is due to the low activation energies for the formation of lactic acid.

This catalytic tendency was also observed for the allylation of benzaldehyde with tetraallyl tin in water (Figure 2).^[22] The yield of 4-phenyl-1-buten-4-ol over various metal triflates is shown in Figure 2. The reaction proceeded even in the absence of an acid catalyst with a yield of about 20% at 303 K for 1 h. Both [Sc(OTf)₃] and [In(OTf)₃] also exhibit high catalytic performance for this reaction with yields of 4-phenyl-1-buten-

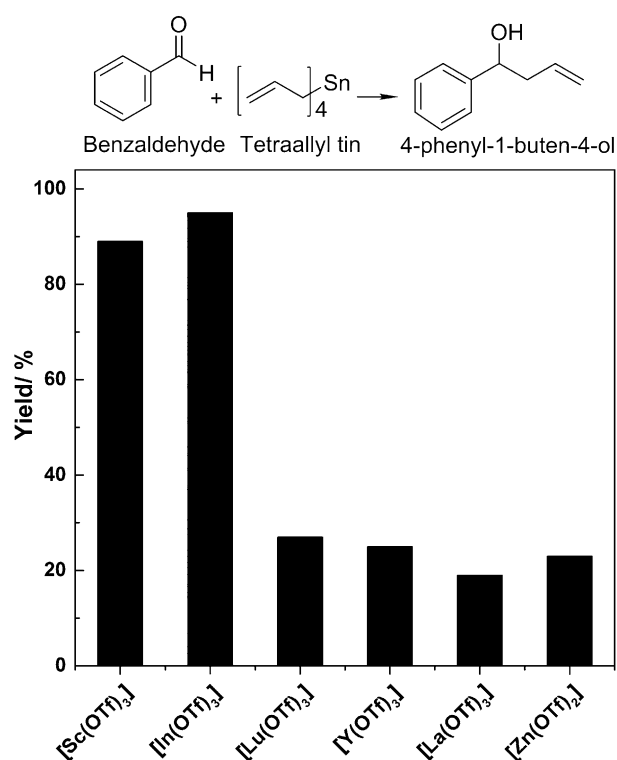


Figure 2. Catalytic activities of metal triflates for the allylation of benzaldehyde with tetraallyl tin in water. Reaction conditions: Catalyst (0.025 mmol), benzaldehyde (0.94 mmol), tetraallyl tin (0.64 mmol), sodium dodecyl sulfate (19.2 mg), water (5 mL), $T = 303$ K, and a reaction time of 1 h.

4-ol that reached 90–95% at 1 h, whereas [Y(OTf)₃], [Lu(OTf)₃], [La(OTf)₃], and [Zn(OTf)₂] afforded product yields of only 20–30%. Taking the results of the blank experiment (without a catalyst) into account, the tested triflates, with the exception of [Sc(OTf)₃] and [In(OTf)₃], are deemed as ineffective catalysts for this reaction. These results demonstrate that [Sc(OTf)₃] and [In(OTf)₃] surpass other triflates in the hydride transfer of pyruvic aldehyde into lactic acid and the allylation of benzaldehyde with tetraallyl tin in water. The high catalytic activity of the scandium and indium complexes has also been reported for other reactions with various carbonyl compounds in water.^[3,5,23] Therefore, the specificity of the Sc³⁺ and In³⁺ sites in metal triflates for the carbonyl compounds contributes to enhance these Lewis acid-catalyzed reactions.

NMR spectroscopic measurement for TMPO–Lewis acid adducts in water

The Lewis acid properties of these metal triflates were evaluated by using ³¹P NMR spectroscopy with TMPO as a basic probe molecule. Activation of a reactant by a Lewis acid is closely related to the energy level of the highest occupied molecular orbital (HOMO) of the reactant (nucleophile) and the lowest unoccupied molecular orbital (LUMO) of the Lewis acid (electrophile).^[1] Thus, a small HOMO/LUMO energy gap means that the nucleophile reacts easily with the Lewis acid to form a stable Lewis acid–nucleophile complex. Density functional theory (DFT) calculations indicated that TMPO has a similar HOMO energy level (–7.2 eV) to those of benzaldehyde (–7.3 eV) and monohydrated pyruvic aldehyde (–7.2 eV), as shown by the energy diagram in Figure 3(a). In addition, the electrons in the HOMO of TMPO are located on the O 2p orbital of the phosphoryl group (Figure 3(b)(i)) as well as the

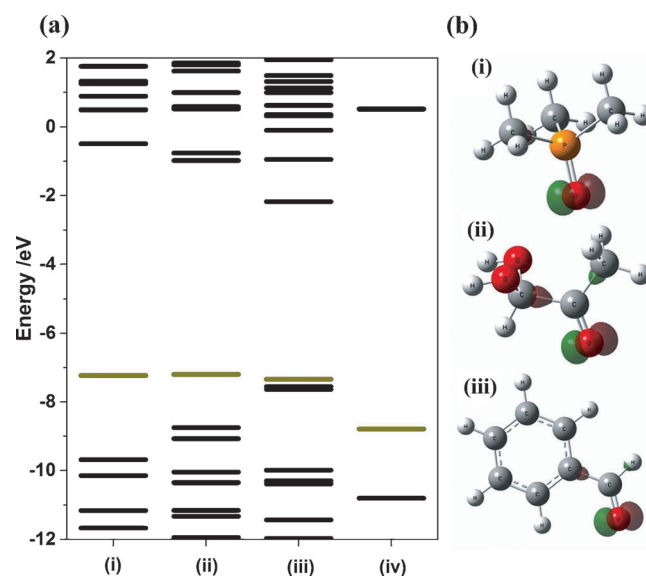


Figure 3. a) HOMO and LUMO energy diagrams for i) TMPO, ii) monohydrated pyruvic aldehyde, iii) benzaldehyde, and iv) water; b) Schematic structure of the HOMOs for i) TMPO, ii) monohydrated pyruvic aldehyde, and iii) benzaldehyde.

HOMO of benzaldehyde and monohydrated pyruvic aldehyde (Figure 3(b)(ii) and (iii)). Such an electronic analogy among TMPO, benzaldehyde, and pyruvic aldehyde indicates that TMPO is a suitable probe molecule for the evaluation of Lewis acid catalysis for these reactions. It should be noted that these substrates, including TMPO, have higher HOMO energies than H₂O (−8.8 eV), which suggests that the Lewis acids react with these molecules in preference to H₂O.

Figure 4 shows ³¹P NMR spectra for TMPO/D₂O solutions with various [Sc(OTf)₃] contents. The intrinsic ³¹P chemical shift

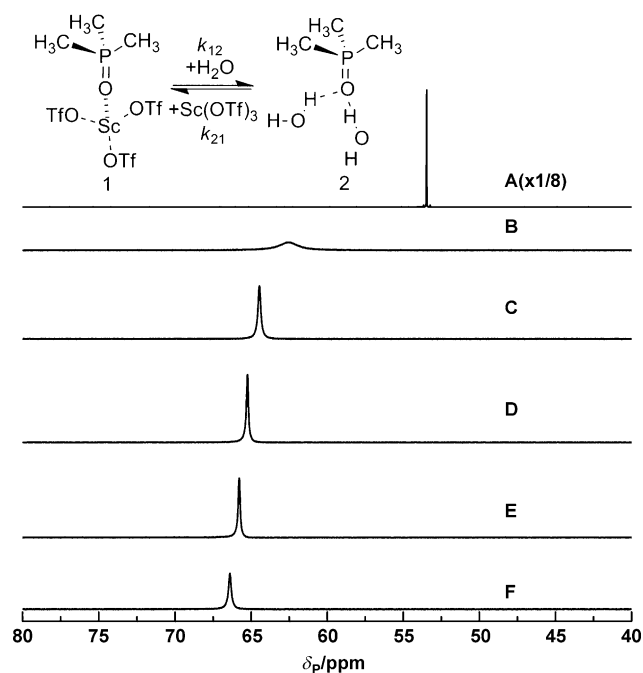


Figure 4. ³¹P NMR spectroscopic measurement of TMPO/D₂O solution (0.25 M) in the presence of various [Sc(OTf)₃] concentrations. Spectrum A: without [Sc(OTf)₃], and spectra B–F show [Sc(OTf)₃]/TMPO ratios of B: 1:2; C: 1:1; D: 2:1; E: 4:1; and F: 8:1.

of TMPO in D₂O solution appears at $\delta = 53.5$ ppm (Figure 4, spectrum A), which is assigned to TMPO interaction with water molecules. After the addition of [Sc(OTf)₃] to the aqueous TMPO solution ([Sc(OTf)₃]/TMPO = 1:2), a resonance peak is observed at $\delta = 62.5$ ppm (Figure 4, spectrum B). This can be explained solely by the formation of the [Sc(OTf)₃TMPO] complex, which is in equilibrium with hydrous TMPO. The single ³¹P NMR spectroscopic peak suggests that the exchange between [Sc(OTf)₃] and D₂O to TMPO proceeds in solution according to the reaction shown in Figure 4. In this case, the peak position of TMPO (Ω_{peak}) is given by the formula with the two chemical shifts shown in the following Equation, in which $[1]_{\text{eq}}$, $[2]_{\text{eq}}$ and Ω_1^0 , Ω_2^0 are the equilibrium concentrations and original chemical shifts of species 1 and 2, respectively.^[24]

$$\Omega_{\text{peak}} = \frac{[1]_{\text{eq}}\Omega_1^0 + [2]_{\text{eq}}\Omega_2^0}{[1]_{\text{eq}} + [2]_{\text{eq}}}$$

The change in chemical shift reflects the change in the equilibrium between these two complexes (Figure 4). The peak position of TMPO continuously shifts to a lower magnetic field with increase in the [Sc(OTf)₃] content. A large downfield chemical shift reflects a significant change in the equilibrium between these two complexes and indicates that most of the TMPO interacts with [Sc(OTf)₃] to form the [Sc(OTf)₃TMPO] complex.

Similar ³¹P NMR spectroscopic measurements were performed for the other metal triflates with various metal triflate/TMPO molar ratios, and the peak positions of the TMPO signals are summarized in Figure 5. The tested metal triflates are

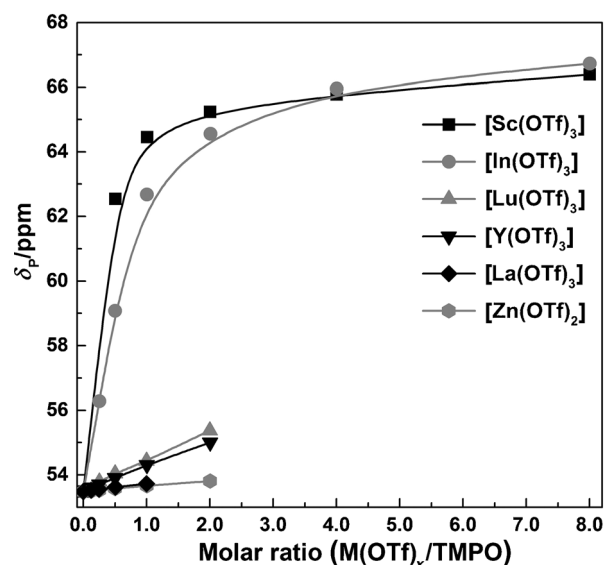


Figure 5. Dependence of TMPO chemical shift in ³¹P NMR spectra on metal triflate/TMPO ratios.

roughly classified into two groups; [Sc(OTf)₃] and [In(OTf)₃], and the other triflates. [Lu(OTf)₃], [Y(OTf)₃], [La(OTf)₃], and [Zn(OTf)₂] exhibit small changes in ³¹P chemical shift and have the TMPO peak at $\delta = 54.4$, 54.3, 53.7, and 53.7 ppm, respectively (metal triflate/TMPO ratio of 1:1). Although the small change in ³¹P chemical shift indicates weak interaction of the Lewis acid center with TMPO, it also means that TMPO on these metal triflates is easily replaced with D₂O in solution. As a result, most TMPO molecules are present in the hydrous form, even at high metal triflate concentrations. In contrast, the TMPO signals for [Sc(OTf)₃] and [In(OTf)₃] are significantly shifted downfield, even with low triflate concentrations (Figure 4 and the Supporting Information, Figure S1a). The TMPO signals for [Sc(OTf)₃] and [In(OTf)₃] appear at $\delta = 64.5$ and 62.7 ppm (metal triflate/TMPO ratio of 1:1) and finally reach $\delta = 66.4$ and 66.7 ppm (metal triflate/TMPO ratio of 8:1), respectively. This large change in the ³¹P chemical shift is derived mainly from the strong affinity of these triflates toward TMPO, even at low concentrations.

It should be noted that the line width of the TMPO resonance in the ³¹P NMR spectra is largely dependent on the metal triflate/TMPO ratio. Although the change in chemical

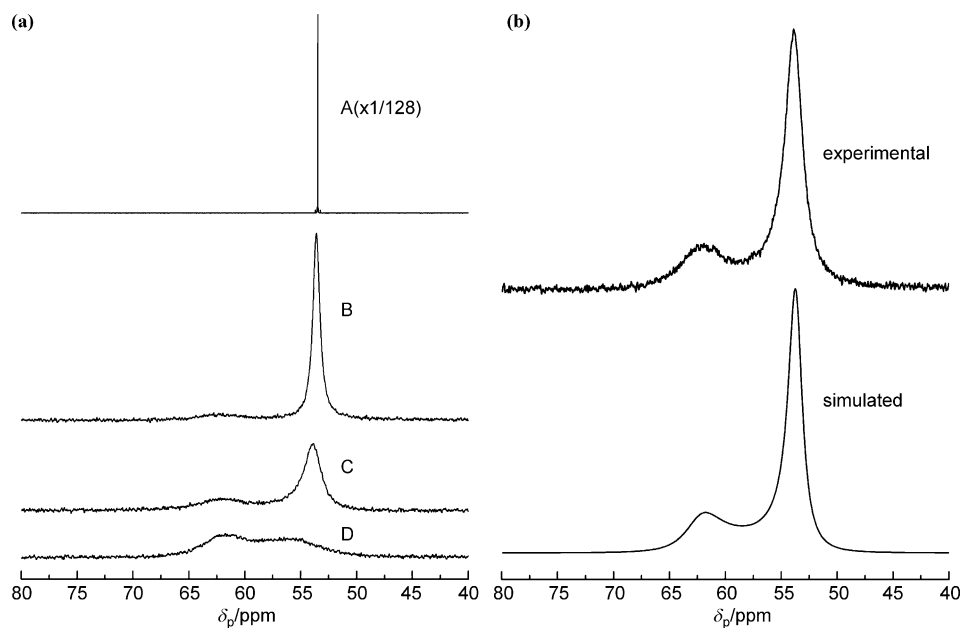
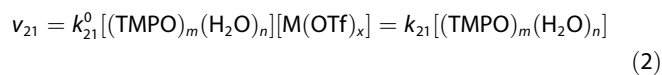
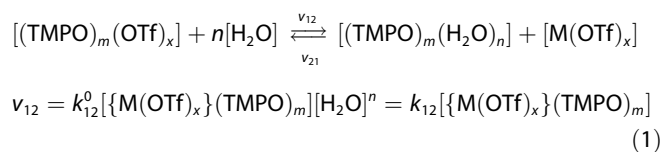


Figure 6. a) ^{31}P NMR spectra of TMPO/ D_2O solution (0.25 M) in the presence of dilute $[\text{Sc}(\text{OTf})_3]$ concentrations. Spectrum A: without $[\text{Sc}(\text{OTf})_3]$, and spectra B–D with triflate/TMPO ratios of B: 1:16, C: 1:8, and D: 1:4; b) experimental and simulated ^{31}P NMR spectra for a $[\text{Sc}(\text{OTf})_3]$ /TMPO ratio of 1:8. The simulated parameters are as follows; $\delta_1 = 62.5$ ppm, $\delta_2 = 53.5$ ppm, $p_1 = 0.28$, $p_2 = 0.72$ and $k_{12} = 2070$ s^{-1} ($k_{21} = 805$ s^{-1}).

shift reflects the presence of the metal triflate–TMPO complex, the line width provides information regarding the exchange rates at micro- to millisecond timescale between metal triflate–TMPO and hydrous TMPO. The ^{31}P NMR spectra for the TMPO/ D_2O solution at lower $[\text{Sc}(\text{OTf})_3]$ concentrations are shown in Figure 6(a). Hydrous TMPO has an intense and sharp resonance at $\delta = 53.5$ ppm, as shown in Figure 6(a), spectrum A. A small increase in the $[\text{Sc}(\text{OTf})_3]$ concentration of the TMPO/ D_2O solution ($[\text{Sc}(\text{OTf})_3]$ /TMPO = 1:16) results in the appearance of two broad signals at around $\delta = 50$ – 55 and 60 – 65 ppm (Figure 6(a), spectrum B). The former and latter signals are assignable to hydrous TMPO and the $[\text{Sc}(\text{OTf})_3\text{TMPO}]$ complex, respectively, and the intensity of the latter signal increases with the $[\text{Sc}(\text{OTf})_3]$ concentration. The line widths of both resonance peaks become broader with an increase in the $[\text{Sc}(\text{OTf})_3]$ concentration. TMPO molecules have interaction with D_2O in solution to form the hydrous state at such low $[\text{Sc}(\text{OTf})_3]$ concentrations; therefore, the broad TMPO resonance can be attributed to the slow exchange rate between $[\text{Sc}(\text{OTf})_3\text{TMPO}]$ and hydrous TMPO. The exchange rates (v_{12} , v_{21}) are given for the following exchange equilibrium:



Here, k_{12} and k_{21} are apparent rate constants that correspond to the ligand exchange rate. Further increase in the $[\text{Sc}(\text{OTf})_3]$ concentration results in a single resonance peak at around $\delta = 65$ ppm (Figure 4), which indicates that most TMPO molecules interact with introduced $[\text{Sc}(\text{OTf})_3]$ to form stable $[\text{Sc}(\text{OTf})_3\text{TMPO}]$ complexes. These ^{31}P NMR spectra with chemical exchange can be simulated according to the chemical shift, peak intensity and ligand exchange rate.^[25] There is no significant difference between the ^{31}P NMR spectrum in Figure 6(a), spectrum C, and that simulated at $\delta_1 = 62.5$ ppm, $\delta_2 = 53.5$ ppm, p_1 (peak intensity of δ_1) = 0.28, p_2 (peak intensity of δ_2) = 0.72, $k_{12} = 2070$ s^{-1} and $k_{21} = 805$ s^{-1} , respectively (Figure 6(b)). Such small k_{12} and k_{21} reflects the slow substitution of D_2O for $[\text{Sc}(\text{OTf})_3]$ on TMPO,^[24,25]

in which 28% of the TMPO molecules form $[\text{Sc}(\text{OTf})_3\text{TMPO}]$ adducts, even at low $[\text{Sc}(\text{OTf})_3]$ concentrations.

The exchange rates of TMPO are also affected by temperature. Figure 7(a) shows ^{31}P NMR spectra for TMPO with $[\text{Sc}(\text{OTf})_3]$ in D_2O ($[\text{Sc}(\text{OTf})_3]$ /TMPO = 1:4) at 278–303 K. The broad and weak signals at $\delta = 63.4$ and 54.8 ppm assigned to $[\text{Sc}(\text{OTf})_3\text{TMPO}]$ and hydrous TMPO, respectively, become sharp and intense with decreasing temperature from 303 to 278 K. The exchange rates of k_{12} and k_{21} were estimated to be 720 and 665 s^{-1} , respectively, from the ^{31}P NMR spectrum at 278 K (Figure 7(a), spectrum A). This directly indicates that the increase in the line widths of the two TMPO resonances is due to slow exchange between $[\text{Sc}(\text{OTf})_3]$ and D_2O on TMPO.

The same experiment was performed for $[\text{In}(\text{OTf})_3]$. Figure 7(b) shows ^{31}P NMR spectra for TMPO with $[\text{In}(\text{OTf})_3]$ in D_2O solution ($[\text{In}(\text{OTf})_3]$ /TMPO = 1:2) at 278–303 K. One broad resonance is observed at 303 K, which gradually splits into two signals ($\delta = 66.0$ and 55.0 ppm) with decrease of the temperature. The k_{12} and k_{21} exchange rates at 278 K were calculated as 2800 and 1575 s^{-1} , respectively. The exchange of TMPO for D_2O in the presence of $[\text{In}(\text{OTf})_3]$ is also slow, as with $[\text{Sc}(\text{OTf})_3]$. In contrast, the ^{31}P NMR spectroscopic signals of TMPO on the other metal triflates ($[\text{Y}(\text{OTf})_3]$, $[\text{Lu}(\text{OTf})_3]$, $[\text{La}(\text{OTf})_3]$, and $[\text{Zn}(\text{OTf})_2]$) have sharp and single resonances at various metal triflate concentrations, as shown in Figure S1 b–e (the Supporting Information), which indicates much faster chemical exchange rates between TMPO and D_2O than those for $[\text{Sc}(\text{OTf})_3]$ and $[\text{In}(\text{OTf})_3]$. The peak widths indicate that these metal triflates, except $[\text{Sc}(\text{OTf})_3]$ and $[\text{In}(\text{OTf})_3]$, undergo chemical exchange at rates above 10^5 s^{-1} , which is much higher than

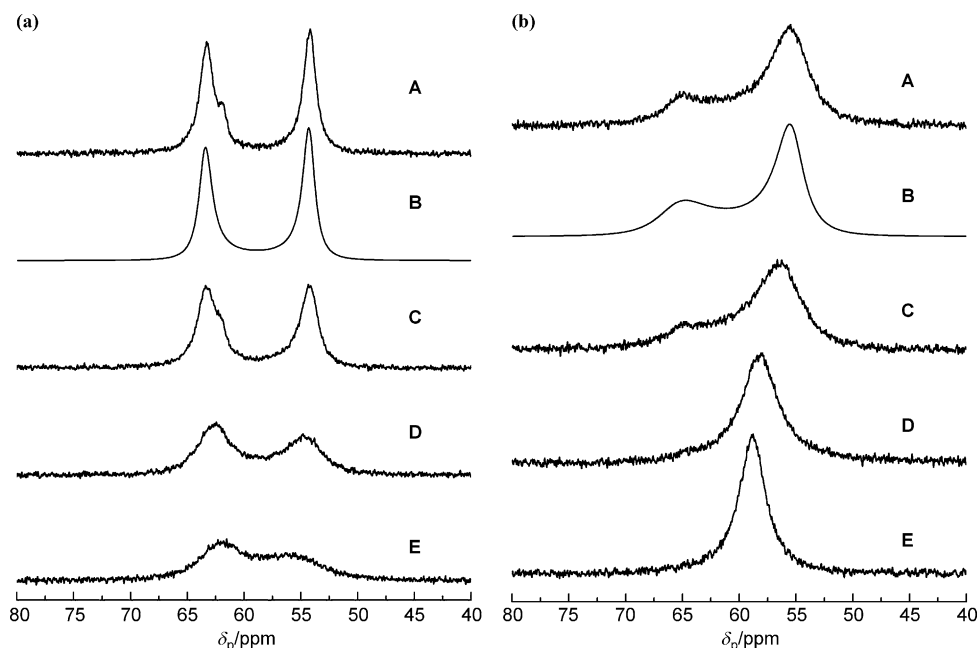


Figure 7. ^{31}P NMR spectra for TMPO/ D_2O solution with a) $[\text{Sc}(\text{OTf})_3]$ ($[\text{Sc}(\text{OTf})_3]/\text{TMPO}=1:4$) and b) $[\text{In}(\text{OTf})_3]$ ($[\text{In}(\text{OTf})_3]/\text{TMPO}=1:2$) at A: 278, C: 283, D: 293, and E: 303 K. Spectrum B is a simulated spectra of A to determine the exchange rates for the two TMPO species (Figure 4). Each parameter was calculated as follows: i) $\delta_1=63.5$ ppm, $\delta_2=54.2$ ppm, $p_1=0.48$, $p_2=0.52$ and $k_{12}=720$ s^{-1} ($k_{21}=665$ s^{-1}) and ii) $\delta_1=66.0$ ppm, $\delta_2=55.0$ ppm, $p_1=0.36$, $p_2=0.64$ and $k_{12}=2800$ s^{-1} ($k_{21}=1575$ s^{-1}).

those for $[\text{Sc}(\text{OTf})_3]$ and $[\text{In}(\text{OTf})_3]$. This is due to the weak coordination of TMPO with the Lewis acid center in water. In addition, the broad resonances of the TMPO signal are not observed when using Brønsted acid catalysts instead.^[13] The chemical exchange rates between TMPO and D_2O over $[\text{Sc}(\text{OTf})_3]$ and $[\text{In}(\text{OTf})_3]$ are therefore much slower than those on the other tested metal triflates, due to the strong Lewis acidity of the metal center. These specific properties of $[\text{Sc}(\text{OTf})_3]$ and $[\text{In}(\text{OTf})_3]$ in water are the main contributing factors to the high catalytic performance for reactions that involve carbonyl compounds. The above correlation of catalytic activity with ^{31}P NMR chemical shifts and spectral shape was also confirmed in metal chlorides such as AlCl_3 , ScCl_3 , YCl_3 , and LaCl_3 (Figure S4, the Supporting Information). AlCl_3 and ScCl_3 with strong interaction with TMPO exhibited much higher catalytic performance than YCl_3 and LaCl_3 .

Quantum chemical calculation of metal triflate–TMPO complexes

The HOMO level of the reactant (nucleophile) and the LUMO level of the Lewis acid (electrophile) are responsible for activation of the reactant with the Lewis acid.^[11] The specific properties of $[\text{Sc}(\text{OTf})_3]$ and $[\text{In}(\text{OTf})_3]$, that is, the high catalytic performance and slow exchange rate between H_2O and reactant over triflates with strong affinity for the reactants, are therefore expected to be due to the LUMO levels of these triflates. To clarify the difference between the high and low catalytic performances among the tested metal triflates, the LUMO energies of the metal triflates were estimated by DFT calculations

after optimization of the metal triflate hydrates based on their crystal structures as model compounds. Trivalent cations in metal triflates have been reported to be stabilized in water with seven to nine water molecules to form a fully coordinated hydrated metal triflate complex, the structure of which is similar to the corresponding metal triflate hydrate crystals (Figure S7, the Supporting Information).^[26,27] Figure 8(a) shows orbital energy diagrams for the Fermi energy regions of six metal triflates. The LUMO energies of $[\text{Sc}(\text{OTf})_3]$ and $[\text{In}(\text{OTf})_3]$ were calculated to be -2.9 and -3.1 eV, respectively, which are considerably lower than the other metal triflates (-1.4 , -1.5 , -1.6 , and -1.7 eV for $[\text{Lu}(\text{OTf})_3]$, $[\text{Y}(\text{OTf})_3]$, $[\text{La}(\text{OTf})_3]$, and $[\text{Zn}(\text{OTf})_2]$, respectively). The LUMOs of $[\text{Sc}(\text{OTf})_3]\cdot 9\text{H}_2\text{O}$ and $[\text{In}(\text{OTf})_3]\cdot 9\text{H}_2\text{O}$ are mainly com-

posed of the outermost shell of each metal cation, as shown in Figure 8(b); the Sc 3d orbital of $[\text{Sc}(\text{OTf})_3]\cdot 9\text{H}_2\text{O}$ and the In 5s orbital of $[\text{In}(\text{OTf})_3]\cdot 9\text{H}_2\text{O}$. Therefore, $[\text{Sc}(\text{OTf})_3]\cdot 9\text{H}_2\text{O}$ and $[\text{In}(\text{OTf})_3]\cdot 9\text{H}_2\text{O}$ act as effective acceptors of electrons from carbonyl oxygen. It is expected from these estimations that $[\text{Sc}(\text{OTf})_3]$ and $[\text{In}(\text{OTf})_3]$ have smaller energy gaps (ΔE) between the LUMO of the metal triflate and the HOMO of the nucleophile than the other metal triflates examined here, which suggests that $[\text{Sc}(\text{OTf})_3]$ and $[\text{In}(\text{OTf})_3]$ can form more stable nucleophile–Lewis acid complexes in water.

The complexation energies of metal triflate–TMPO and metal triflate–monohydrated pyruvic aldehyde complexes (ΔE_{c}), and the interatomic distances between the metal cation and phosphoryl or carbonyl oxygen (R_{MO}) were also evaluated with respect to DFT calculations. Also in these calculations, it was demonstrated that $[\text{Sc}(\text{OTf})_3]$ and $[\text{In}(\text{OTf})_3]$ are capable of forming much more stable complexes with TMPO and pyruvic aldehyde than other metal triflates (Table S1, the Supporting Information). Thus, strong interaction between the metal cation and the carbonyl oxygen is necessary for effective electron donation from the carbonyl substrate to the Lewis acid catalyst.

Conclusion

Changes in the ^{31}P NMR chemical shift and line width of TMPO–Lewis acid complexes in water are effective for evaluation of the catalytic performance of water-tolerant Lewis acids for reactions involving carbonyl groups in water. The higher catalytic performance of $[\text{Sc}(\text{OTf})_3]$ and $[\text{In}(\text{OTf})_3]$ compared

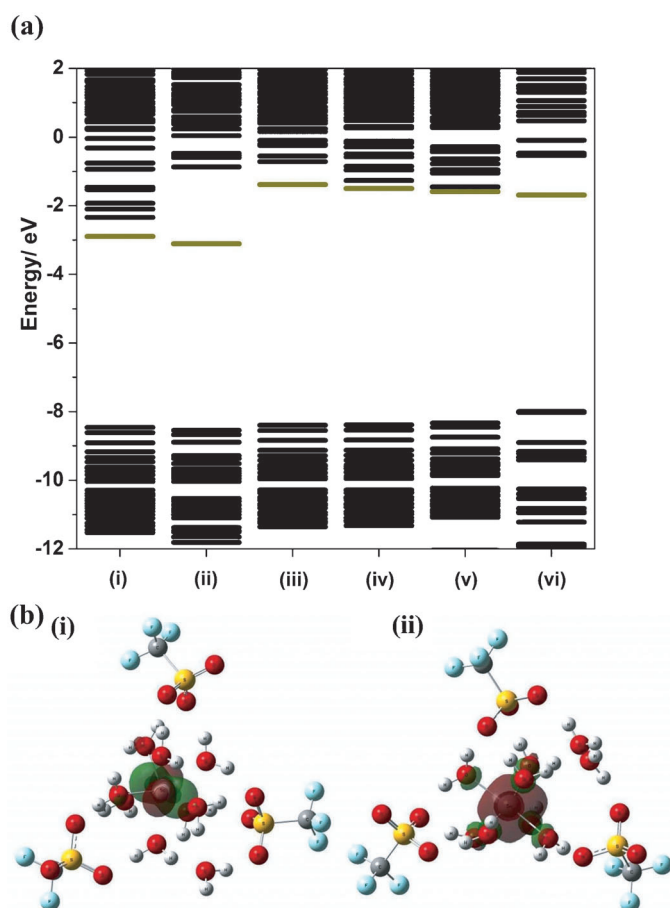


Figure 8. a) HOMO and LUMO energy diagrams for i) [Sc(OTf)₃]-9H₂O, ii) [In(OTf)₃]-9H₂O, iii) [Lu(OTf)₃]-9H₂O, iv) [Y(OTf)₃]-9H₂O, v) [La(OTf)₃]-9H₂O, and vi) [Zn(OTf)₂]-6H₂O; b) schematic structure of the LUMOs for i) [Sc(OTf)₃]-9H₂O and ii) [In(OTf)₃]-9H₂O. The central atoms of i) and ii) are Sc and In, respectively.

with the other triflates examined here is due to the formation of stable nucleophile–Lewis acid complexes in water, resulting in the considerably slow reactant–water exchange of [Sc(OTf)₃] and [In(OTf)₃] (Figure 9). The low LUMO energies of [Sc(OTf)₃] and [In(OTf)₃] estimated by DFT calculations supported the conclusions made from ³¹P NMR spectroscopic measurements with TMPO. Efficient activation of carbonyl groups in the reac-

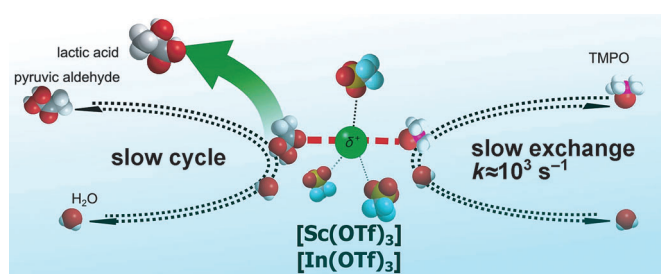


Figure 9. Schematic image of the correlation between pyruvic aldehyde and TMPO over [Sc(OTf)₃] and [In(OTf)₃] catalysts.

tant by the Lewis acid is important to achieve high catalytic performance for Lewis acid-catalyzed reactions.

Experimental Section

Materials

[Sc(OTf)₃], [In(OTf)₃], [Lu(OTf)₃], [Y(OTf)₃], [La(OTf)₃], and [Zn(OTf)₂] were obtained from Aldrich. Prior to NMR spectroscopic measurements and catalytic reaction experiments, the metal triflates were dehydrated at 423 K for 3 h under vacuum to remove physisorbed water. AlCl₃ (High Purity Materials), [ScCl₃]-6H₂O (Strem Chemicals Inc.), YCl₃ (Strem Chemicals Inc.) and [LaCl₃]-7H₂O (Wako) were also tested as received.

Catalytic reactions

Catalytic reactions with the metal triflates were tested through the hydride transfer of pyruvic aldehyde into lactic acid and the allylation of benzaldehyde with tetraallyl tin in water. The former reaction was conducted by heating a sealed Pyrex tube containing a mixture of catalyst (0.1 mmol) and 0.1 M aqueous pyruvic aldehyde (2.0 mL) at 323–403 K. The reactant solutions were analyzed by using high performance liquid chromatography (HPLC) with a refractive index (RI) detector. For the allylation of benzaldehyde with tetraallyl tin in water, a mixture of catalyst (0.025 mmol), benzaldehyde (0.94 mmol), tetraallyl tin (0.64 mmol), sodium dodecyl sulfate (19.2 mg), and water (5 mL) was kept at 303 K for 1 h. Sodium dodecyl sulfate was used as a surfactant that solubilizes hydrophobic organic reactants and forms an emulsion in water. The product was extracted from solution with ethyl acetate and analyzed by using gas chromatography (GC).

NMR spectroscopic measurements

The interaction of Lewis acids with TMPO in water was evaluated by using ³¹P NMR spectroscopy (Bruker AVANCE III 400) at resonance frequencies of 400.1 and 162.0 MHz for ¹H and ³¹P, respectively. Each catalyst was dissolved in a solution of TMPO/D₂O (0.25 M). The Lewis acidities of the metal triflates were compared according to the chemical shift and line width of the NMR spectral peaks. ³¹P NMR spectroscopic measurements were performed at 303 K under ¹H decoupling to remove the influence of ¹H-³¹P spin-spin coupling. The number of scans and recycle delay were set at 32 and 128 times and 5 s, respectively. The ³¹P chemical shift was referenced using the 0.25 M TMPO/D₂O solution at 53.50 ppm as an external standard relative to 85% H₃PO₄ aq. at $\delta = 0$ ppm.

Quantum chemical calculations

All calculations were performed with the B3LYP density functional,^[28] as implemented in the Gaussian 09 software.^[29] Calculations for TMPO, monohydrated pyruvic aldehyde, benzaldehyde and water, were conducted using 6-311+G(d,p) basis set. In the calculations of metal complexes, the structure of the metal triflates involving trivalent cations (Sc³⁺, In³⁺, Lu³⁺, Y³⁺, and La³⁺) were referenced to a single molecular unit extracted from the crystal structure of [Sc(OTf)₃]-9H₂O.^[26] After the optimization of [Sc(OTf)₃]-9H₂O, the metal cation was changed from Sc³⁺ to In³⁺, Lu³⁺, Y³⁺, or La³⁺ and each metal triflate hydrate was optimized again. The structure of [Zn(OTf)₂] was also optimized based on a molecular unit extracted from the crystal structure of [Zn(OTf)₂]-6H₂O.^[30] The complexes of metal triflate–TMPO and metal triflate–monohydrated pyruvic aldehyde were also calculated after placing a TMPO and monohy-

drated pyruvic aldehyde molecule in the vacant space of the optimized metal triflate hydrate. Calculations of the metal triflates and triflate complexes were performed with the CEP-121G^[31] and 6-311+G(d,p) basis sets for the metal cation and other atoms, respectively. Contour maps for the HOMOs and LUMOs were constructed by using the GaussView software.^[32]

Acknowledgements

The authors thank Y. Sei at the Material Analysis Suzukake-dai Center of the Tokyo Institute of Technology for significant discussions regarding NMR spectroscopic analysis. We also thank the Cambridge Crystallographic Data Centre (CCDC) for the use of CIF files for the metal triflate hydrates as references for the DFT calculations.

Keywords: carbonyl compounds · density functional calculations · Lewis acids · metal triflates · NMR spectroscopy

- [1] A. Corma, H. García, *Chem. Rev.* **2003**, *103*, 4307–4365.
- [2] a) D. Schinzer, *Selectivities in Lewis Acid Promoted Reactions*, Kluwer Academic Publishers, Dordrecht, **1989**; b) H. Yamamoto, *Lewis Acids in Organic Synthesis*, Wiley-VCH, Weinheim, **2000**.
- [3] a) S. Kobayashi, S. I. Hachiya, *J. Org. Chem.* **1994**, *59*, 3590–3596; b) S. Kobayashi, K. Manabe, *Acc. Chem. Res.* **2002**, *35*, 209–217; c) S. Kobayashi, C. Ogawa, *Chem. Eur. J.* **2006**, *12*, 5954–5960.
- [4] S. Kobayashi, T. Wakabayashi, S. Nagayama, H. Oyamada, *Tetrahedron Lett.* **1997**, *38*, 4559–4562.
- [5] a) S. Kobayashi, *Eur. J. Org. Chem.* **1999**, 15–27; b) S. A. Cotton, *Polyhedron* **1999**, *18*, 1691–1715; c) K. Manabe, Y. Mori, T. Wakabayashi, S. Nagayama, S. Kobayashi, *J. Am. Chem. Soc.* **2000**, *122*, 7202–7207.
- [6] Y. Román-Leshkov, M. E. Davis, *ACS Catal.* **2011**, *1*, 1566–1580.
- [7] S. Kobayashi, S. Nagayama, T. Busujima, *J. Am. Chem. Soc.* **1998**, *120*, 8287–8288.
- [8] H. Tsuruta, K. Yamaguchi, T. Imamoto, *Tetrahedron* **2003**, *59*, 10419–10438.
- [9] a) F. Wang, C. Liu, W. Dong, *Green Chem.* **2013**, *15*, 2091–2095; b) F. Wang, A. Shi, X. Qin, C. Liu, W. Dong, *Carbohydr. Res.* **2011**, *346*, 982–985.
- [10] Y. Jiang, J. Huang, W. Dai, M. Hunger, *Solid State Nucl. Magn. Reson.* **2011**, *39*, 116–141.
- [11] A. Zheng, S. J. Huang, S. B. Liu, F. Deng, *Phys. Chem. Chem. Phys.* **2011**, *13*, 14889–14901.
- [12] Y. Chu, Z. Yu, A. Zheng, H. Fang, H. Zhang, S. J. Huang, S. B. Liu, F. Deng, *J. Phys. Chem. C* **2011**, *115*, 7660–7667.
- [13] C. Y. Yang, Z. Yu, A. Zheng, H. Fang, H. Zhang, S. J. Huang, S. B. Liu, F. Deng, *J. Anal. Sci. Technol.* **2011**, *2*, A155–A158.
- [14] R. M. West, M. S. Holm, S. Saravanamurugan, J. Xiong, Z. Beversdorf, E. Taarning, C. H. Christensen, *J. Catal.* **2010**, *269*, 122–130.
- [15] M. S. Holm, S. Saravanamurugan, E. Taarning, *Science* **2010**, *328*, 602–605.
- [16] E. Taarning, S. Saravanamurugan, M. S. Holm, J. Xiong, R. M. West, C. H. Christensen, *ChemSusChem* **2009**, *2*, 625–627.
- [17] Y. Hayashi, Y. Sasaki, *Chem. Commun.* **2005**, 2716–2718.
- [18] M. Dusselier, P. V. Wouwe, A. Dewaele, E. Makshina, B. F. Sels, *Energy Environ. Sci.* **2013**, *6*, 1415–1442.
- [19] a) P. Y. Dapsens, C. Mondelli, J. Perez-Ramirez, *ACS Catal.* **2012**, *2*, 1487–1499; b) R. M. Painter, D. M. Pearson, R. M. Waymouth, *Angew. Chem.* **2010**, *122*, 9646–9649; *Angew. Chem. Int. Ed.* **2010**, *49*, 9456–9459.
- [20] Y. Román-Leshkov, M. Moliner, J. A. Labinger, M. E. Davis, *Angew. Chem.* **2010**, *122*, 9138–9141; *Angew. Chem. Int. Ed.* **2010**, *49*, 8954–8957.
- [21] Y. Koito, K. Nakajima, M. Kitano, M. Hara, *Chem. Lett.* **2013**, *42*, 873–875.
- [22] G. E. Keck, K. H. Tarbet, L. S. Geraci, *J. Am. Chem. Soc.* **1993**, *115*, 8467–8468.
- [23] a) H. Yamamoto, K. Oshima, *Main Group Metals in Organic Synthesis*, Wiley-VCH, Weinheim, **2005**; b) A. Kawata, K. Tanaka, Y. Kuninobu, K. Takai, *Angew. Chem.* **2007**, *119*, 7939–7941; *Angew. Chem. Int. Ed.* **2007**, *46*, 7793–7795; c) R. Ghosh, S. Malti, *J. Mol. Catal. A* **2007**, *264*, 1–8.
- [24] M. H. Levitt, *Spin dynamics*, 2nd ed., Wiley, Chichester, **2008**, pp. 516–527.
- [25] J. L. Sudmeier, J. L. Evelhoch, N. B. H. Jonsson, *J. Magn. Reson.* **1980**, *40*, 377–390.
- [26] A. Abbasi, P. Lindqvist-Reis, L. Eriksson, D. Sandström, S. Lidin, I. Persson, M. Sandström, *Chem. Eur. J.* **2005**, *11*, 4065–4077.
- [27] a) J. Näslund, P. Lindqvist-Reis, I. Persson, M. Sandström, *Inorg. Chem.* **2000**, *39*, 4006–4011; b) T. Yamaguchi, M. Niihara, T. Takamuku, H. Wakita, H. Kanno, *Chem. Phys. Lett.* **1997**, *274*, 485–490.
- [28] a) A. D. Becke, *Phys. Rev. A* **1988**, *38*, 3098–3100; b) C. Lee, W. Yang, R. G. Parr, *Phys. Rev. B* **1988**, *37*, 785–789; c) A. D. Becke, *J. Chem. Phys.* **1993**, *98*, 1372–1377; d) A. D. Becke, *J. Chem. Phys.* **1993**, *98*, 5648–5652.
- [29] Gaussian 09, Revision C.01, M. J. Frisch, G. W. Trucks, H. B. Schlegel, G. E. Scuseria, M. A. Robb, J. R. Cheeseman, G. Scalmani, V. Barone, B. Menonucci, G. A. Petersson, H. Nakatsuji, M. Caricato, X. Li, H. P. Hratchian, A. F. Izmaylov, J. Bloino, G. Zheng, J. L. Sonnenberg, M. Hada, M. Ehara, K. Toyota, R. Fukuda, J. Hasegawa, M. Ishida, T. Nakajima, Y. Honda, O. Kitao, H. Nakai, T. Vreven, J. A. Montgomery, Jr., J. E. Peralta, F. Ogliaro, M. Bearpark, J. J. Heyd, E. Brothers, K. N. Kudin, V. N. Staroverov, R. Kobayashi, J. Normand, K. Raghavachari, A. Rendell, J. C. Burant, S. S. Iyengar, J. Tomasi, M. Cossi, N. Rega, J. M. Millam, M. Klene, J. E. Knox, J. B. Cross, V. Bakken, C. Adamo, J. Jaramillo, R. Gomperts, R. E. Stratmann, O. Yazyev, A. J. Austin, R. Cammi, C. Pomelli, J. W. Ochterski, R. L. Martin, K. Morokuma, V. G. Zakrzewski, G. A. Voth, P. Salvador, J. J. Dannenberg, S. Dapprich, A. D. Daniels, Ö. Farkas, J. B. Foresman, J. V. Ortiz, J. Cioslowski, D. J. Fox, Gaussian, Inc., Wallingford CT, **2009**.
- [30] C. Nguyen-Trung, J. C. Bryan, D. A. Palmer, *Struct. Chem.* **2004**, *15*, 89–94.
- [31] a) W. J. Stevens, M. Krauss, H. Basch, P. G. Jasien, *Can. J. Chem.* **1992**, *70*, 612–630; b) T. R. Cundari, W. J. Stevens, *J. Chem. Phys.* **1993**, *98*, 5555–5565.
- [32] R. Dennington, T. Keith, J. Millam, GaussView, Version 5, Semichem Inc., Shawnee Mission KS, **2009**.

Received: January 21, 2014

Revised: April 4, 2014

Published online on May 26, 2014